Measurement and analysis of internal stress distributions created in gelatin simulated-brain tissue by a pulsed laser-induced liquid jet*

T. Kato, T. Arafune, T. Washio, A. Nakagawa, Y. Ogawa, T. Tominaga, I. Sakuma, and E. Kobayashi

Abstract— **Transsphenoidal surgery is currently employed to treat complex lesions beyond the sella turcica; however, the procedure can be limited by difficulties encountered in dealing with small blood vessels, deep and narrow working spaces, and awkward working angles. To overcome these problems, we have developed a pulsed laser-induced liquid jet system that can dissect tumor tissue while preserving fine blood vessels within deep and narrow working spaces. We have previously evaluated the utility and safety of this procedure. However, the effects of the pulsejet after being injected into the brain are not yet well understood. Especially, the behavior of the stress distribution created by the jet is important because it has recently been reported that high acoustic pressures can affect the brain. In this study, we measured internal stress distributions in a gelatin simulated-brain using photoelasticity experiments. We used a high-speed camera with an image sensor on which an array of micropolarizers was attached to measure the stresses and the shear wave created when the pulsejet enters the simulated brain.**

I. Introduction

To date, surgical operations are expected to not only result in high survival rates but also involve minimum invasiveness with maximum preservation of functionality. Medical technology is also expected to respond sensitively to drastic changes in insurance systems and to the requirements of an aging society.

Our research has been aimed at developing a laser-induced liquid jet (LILJ) system to dissect tumor tissues while preserving fine blood vessels within deep and narrow working spaces; we have also been evaluating the utility and safety of the LILJ system. The jet energy source is a pulsed holmium:yttrium-aluminum-garnet (Ho:YAG) laser system (Mid-Infrared Pulse Laser System; Sparkling Photon, Inc., Tokyo, Japan) with a wavelength of 2.1 μm and a pulse duration of 350 μs. The energy of the laser can be varied from 300 to 500 mJ per pulse, and the pulse rate can be varied from 1 to 10 Hz. The efficacy and safety of the LILJ have been demonstrated in previous studies [1].

Unlike other devices, the LILJ has the ability to incise, exfoliate, and crush body tissues simultaneously. Consequently, the LILJ has allowed us to reduce operating times and total blood losses while improving outcomes in the difficult neurosurgery of pituitary tumors [2].

The LILJ injects a jet at a velocity of about 10 m/s into the brain and stresses brain tissue around the injection point. Recently, an effect of high acoustic pressure on brain tissue has been reported [3]; therefore, we must understand how the internal stress distribution created by a liquid jet impacts the brain, which is the purpose of this research. In this study, we used photoelasticity experiments to measure the stress distribution in a gelatin simulated-brain and discuss the measured stresses and shear waves.

II. Materials and Methods

A photoelasticity experiment is a method for measuring internal stress distributions in a material that has photoelasticity [4]. When a photoelastic material is stressed, it behaves like a birefringent crystal. Therefore, if linearly polarized light is injected into the stressed material, the transmitted light is composed of both ordinary light and extraordinary light because of birefringence. Thus, by using a polarizer to block the ordinary light, we can measure the stress distribution.

Such a photoelastic experiment can measure isoclinic and isochromatic lines. Isoclinic lines represent contours along which the orientation of the principal stress direction is constant. However, isochromatic lines represent contours along which the difference in the principal stresses on the image plane is a constant. In our experiments, we measured isoclinic lines to understand the stress distribution around the tip of the jet pulse and isochromatic lines to detect shear wave fronts.

A. Method of measuring isochromatic lines

Fig. 1 shows the components used in a photoelasticity experiment for measuring isochromatic lines. We used a green laser (λ = 532 nm) (Fig. 1(a)). First, we created linearly polarized light using the polarizer (Fig. 1(b)) and circularly polarized light using a quarter wavelength plate (Fig. 1(c)). Second, photoelasticity of the gelatin target (5 wt%, 10°C) (Fig. 1(d)) introduced a phase difference in the circularly polarized light. Finally, using a quarter wavelength plate (Fig. 1(e)) and analyzer (Fig. 1(f)), we measured isochromatic lines. The extraordinary light generated by the gelatin target was

*This study is (partially) funded by Ministry of Economy, Trade and Industry, Japan as a part of "Program to support collaboration between hospitals and businesses for development and improvement of medical equipment and devices to solve unmet medical needs (supplementary budget, 2010 FY).

T. Kato, I. Sakuma, and E. Kobayashi are with School of Engineering, The University of Tokyo, 113-8656 Tokyo, Japan (e-mail: kato@bmpe.t.u-tokyo.ac.jp, sakuma@bmpe.t.u-tokyo.ac.jp, etsuko@bmpe.t.u-tokyo.ac.jp).

T. Arafune is with Graduate School of Science and Engineering, Tokyo Denki University, 350-0394 Saitama, Japan (e-mail: arafune.t@mail.dendai.ac.jp).

T. Washio is with The National Institute of Advanced Industrial Science and Technology, 305-8564 Tsukuba, Japan (e-mail: washio.t@aist.go.jp).

A. Nakagawa and T. Tominaga are with Department of Neurosurgery, Tohoku University, Graduate School of Medicine, 980-8577 Sendai, Japan (e-mail: nakg_neurosurg@yahoo.co.jp).

Y. Ogawa is with Department of Neurosurgery, Kohnan Hospital, 982-8523 Sendai, Japan (e-mail: yogawa@kohnan-sendai.or.jp).

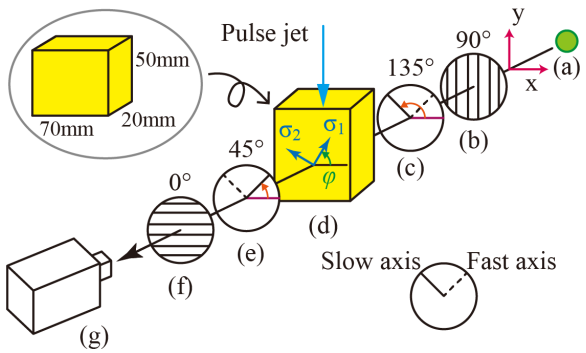

Figure 1. Components in the photoelasticity experiment for measuring isochromatic lines. Components include (a) laser source (532 nm), (b) polarizers, (c) and (e) quarter wavelength plates, (d) gelatin target, (f) analyzer, and (g) high-speed camera. φ is the isoclinic angle or the angle of σ_1 with respect to the x-axis in (d).

captured by a high-speed camera (FASTCAM SA4, Photron, Japan) at a recording speed of 30,000 fps.

We used Jones calculus to deduce a relation between the phase differences of photoelasticity and transmitted light intensity. In Fig. 1, when the Jones vector of linearly polarized light created by the polarizer is written as $\mathbf{E} = [E_x\ E_y]^{\mathrm{T}} = [0\ 1]^{\mathrm{T}}$, the light vector passed to the analyzer is given by,

$$\begin{bmatrix} E_x \\ E_y \end{bmatrix} = \begin{bmatrix} \sin(\delta/2)\exp(-i2\varphi) \\ 0 \end{bmatrix}, \tag{1}$$

where the phase difference δ is given by,

$$\delta = (2\pi h/\lambda)(\sigma_1 - \sigma_2). \tag{2}$$

In (2), σ_1 and σ_2 are the principle stresses on the x–y plane and h is the thickness of the gelatin target. Equation (2) indicates that δ is proportional to the principle shear stress. The intensity of light, $I_d = E_x E_x^*$, is obtained from (1) as

$$I_d = I_a \sin^2(\delta/2), \tag{3}$$

where I_a accounts for the intensity of the laser source. Equation (3) shows that the measured light intensity depends only on δ; thus, the high-speed camera measures the stress distribution via light intensity. However, the stress distribution generated by the pulsejet is not isotropic in three dimensions. Therefore, the thickness h is not constant and δ in (3) must be integrated over h. However, we can measure a boundary of the stress distribution shortly after the pulsejet is injected. The shear wave is the propagation of the stress; thus, the wave front can be detected.

B. Method of measuring isoclinic lines

The photoelasticity apparatus in Fig. 1 can measure isochromatic lines using a high-speed camera. However, an isochromatic line only accounts for the difference in the principal stresses on the image plane. To measure isoclinic lines, we need to change the orientation of the analyzer. Moreover, the stress distribution in the gelatin target is not a constant distribution, and the apparatus in Fig. 1 cannot measure dynamic isoclinic lines.

To overcome this problem, we use a high-speed camera that has an image sensor on which an array of micropolarizers is attached [5] (Photron, Japan). Fig. 2 shows the components in the photoelasticity experiment for measuring isoclinic lines,

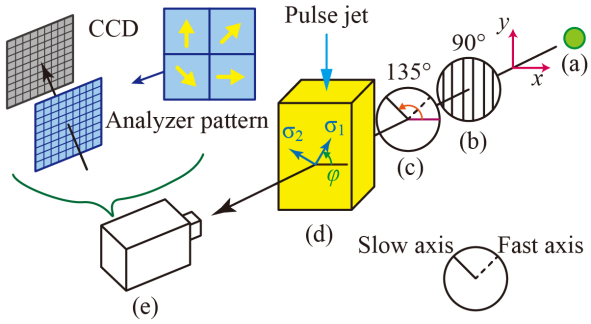

Figure 2. Components in the photoelasticity experiment for measuring isoclinic lines. Components include (a) laser source (532 nm), (b) polarizers, (c) quarter wavelength plate, (d) gelatin target, (e) high-speed camera that has an image sensor on which an array of micropolarizers was attached. φ is the isoclinic angle or the angle of σ_1 with respect to the x-axis in (d).

including the high-speed camera. Because of the array of micropolarizers, the high-speed camera has an analyzer pattern in four directions (Fig. 2(e)). The analyzer, which was made of photonic crystal, was attached to each pixel of the CCD. On four pixels, 2 × 2 pixels, the directions of analyzers were 0°, 45°, 90°, and 135°. We assume that these pixels provided information on one point of the target. Therefore, using the high-speed camera with micropolarizers, we can measure isoclinic lines around four analyzer angles at one time and determine the isoclinic angle.

Tobita et al. determined the isoclinic angle, φ in Fig. 2 (d), using a high-speed camera with micropolarizers [6]. Let I_1, I_2, I_3 and I_4 be the measured light intensities on the CCD with an attached analyzer pattern whose directions are 0°, 45°, 90°, and 135°. Then, the isoclinic angle is given by,

$$\varphi = \frac{1}{2}\arctan\{(I_3 - I_1)/(I_2 - I_4)\}, \tag{4}$$

For the apparatus in Fig. 2, the light intensities in (4) were obtained from the three-dimensional stress distribution. Therefore, the stress distribution cannot be directly analyzed from only the results of the experiment for isoclinic lines.

C. Integrated isochromatic and isoclinic angles

In this section, we develop the equation for determining integrated isochromatic and isoclinic angles. Fig. 3 shows a conceptual diagram of digital photoelasticity for comparing isoclinic lines. The propagation of a polarized light ray in the direction of the z-axis through an elastically deformed photoelastic medium under an arbitrary 3D stress is governed by [7]

$$d\mathbf{A}/dz = \mathbf{GA}, \tag{8}$$

where the transformation matrix, which gives the effect of photoelasticity in dz, is

$$\mathbf{G} = -iC_0/2\begin{bmatrix} \sigma_{11} - \sigma_{22} & 2\sigma_{12} \\ 2\sigma_{12} & \sigma_{22} - \sigma_{12} \end{bmatrix}, \tag{9}$$

and the light vector $\mathbf{A} = \{A_1\ A_2\}^{\mathrm{T}}$.

The light vector $\mathbf{A}^{(i)}$ and the transformation matrix $\mathbf{G}^{(i)}$ are at z_i $(i = 0 \ldots n)$. The light vectors $\mathbf{A}^{(i-1)}$ and $\mathbf{A}^{(i)}$ are input and output light vectors for the ith element (Fig. 3). Then, the final output light $\mathbf{A}^{(n)}$ can be expressed as follows:

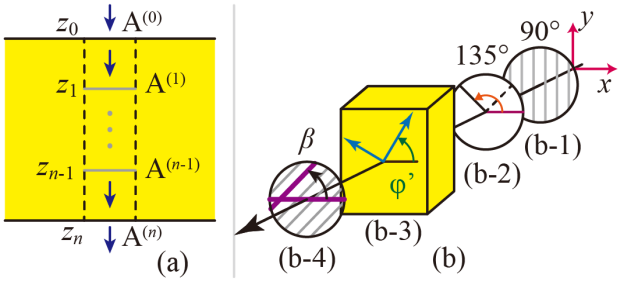

Figure 3. Conceptual diagram for digital photoelasticity used to compare isoclinic lines. (a) Scheme of calculating light vectors **A**. (b) Process of digital photoelasticity. (b-3) φ' is the integrated isoclinic angle with respect to the *x*-axis.

$$\mathbf{A^{(n)}} = \left(\mathbf{I} + \mathbf{H}^{(n)}\right) \cdots \left(\mathbf{I} + \mathbf{H}^{(2)}\right)\left(\mathbf{I} + \mathbf{H}^{(1)}\right)\mathbf{A^{(0)}}, \qquad (10)$$

where **I** is a 2 × 2 identity matrix and $\mathbf{H}^{(i)} = \mathbf{G}^{(i)}(z_i - z_{i-1})$.

If we consider the light vector **A** as a Jones vector, the final output light can be obtained from (10) following the methodology used to deduce (1). Using the integrated isoclinic angle φ' (Fig. 3(b-2)) and the integrated phase difference δ', the intensity of the final light vector I_β when the incident light vector is $\mathbf{A} = [0\ 1]^T$ (Fig. 3(b-1)) and the analyzer angle is β (Fig. 3(b-3)) is given by,

$$I_\beta = I_a + I_0 \sin 2\left(\beta - \varphi'\ \right), \qquad (11)$$

where I_a and I_0 are constants. Substituting $\beta = 0, \pi/4, \pi/2,$ and $3\pi/4$ in (11), we obtain the intensities I_1, I_2, I_3, and I_4. This process is the same as that in Fig. 2; thus, the integrated isoclinic angle φ' can be obtained from (4). Axial symmetry of the pulsejet indicates that the stress distribution is also axially symmetrical. We consider the directions of internal principle stresses based on this symmetry.

The power of the LILJ used in the experiment was 0.8 kV, yielding a velocity of the pulsejet of 10 m/s. To make the pulsejet visible, we used lactated Ringer's solution and added ink to the solution. We injected the pulsejet and measured data at twelve subsequent times after injection.

III. Results

Fig. 4 shows an isochromatic line of gelatin compressed by the pulsejet. Each panel in the figure shows the difference between each video frame and the first frame (t = 0 ms). The panels show propagation of the shear wave. The isochromatic line represents the integrated internal stress distribution. Therefore, the intensity of light, integrated over the isochromatic line, gives the relative intensity of internal stress on the image plane. In the panels, the blue regions are the regions of the pulsejet because ink was mixed with the pulsejet, which blocked the light.

Fig. 5 shows the isoclinic line in gelatin compressed by the pulsejet. The integrated isoclinic angle in these panels is about 120° because residual stresses and small optical errors easily created phase differences. These panels show the isoclinic line at the time when the pulsejet was injected. To show the region of the pulsejet, we created a mask for the raw CCD image by using ink to block light from the region of the pulsejet on the image.

IV. Discussion

Fig. 4 shows that the pulsejet generates a shear wave in the target. A shear wave is generated because the pulsejet impacts the gelatin target as it enters. In the direction of the axis perpendicular to the flow of the pulsejet (direction β in Fig. 4), the figure shows that the pulsejet generated a small

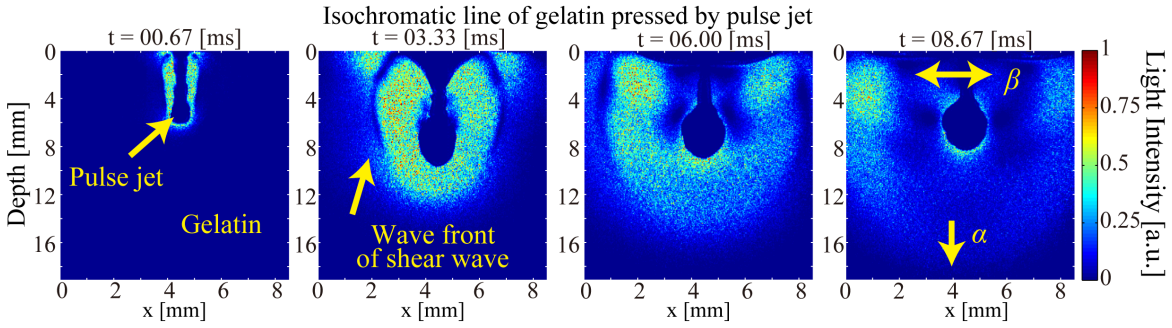

Figure 4. Isochromatic line of gelatin compressed by pulsejet. Panels show the isochromatic line at selected times after the pulsejet was injected. α and β indicate directions parallel to the flow of the pulsejet and perpendicular to the flow, respectively.

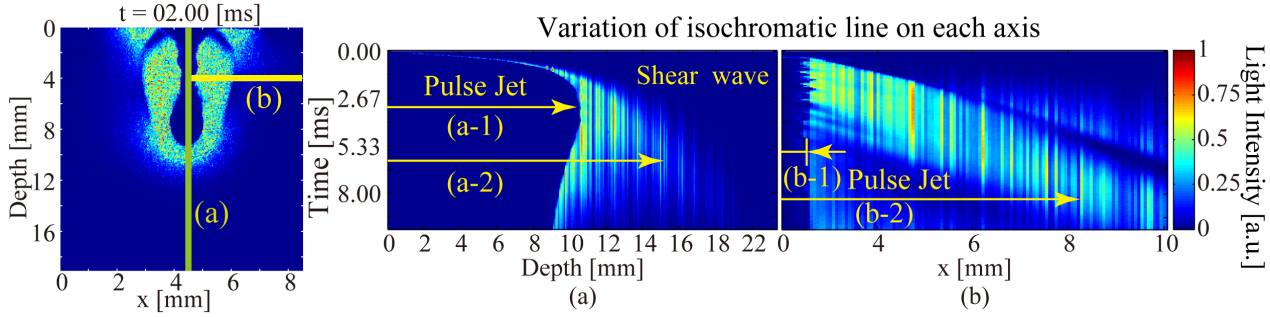

Figure 5. Variations in the isoclinic line on each axis. These panels show time variations in isochromatic line on (a) the centerline of the pulsejet and (b) the horizontal axis perpendicular to the pulsejet. Zero positions in (a) and (b) refer to the surface of gelatin and the centerline of the pulsejet, respectively. In Panels (a) and (b), (a-1) and (b-1) are reaching distances of the pulsejet, while (a-2) and (b-2) are distances to positions at which the light intensity was $1/e$.

TABLE 1. PROPAGATION DISTANCE OF THE SHEAR WAVE.

	Reaching distance of the pulsejet (a) [mm]	*Propagation distance (b) [mm]*	*(b)/(a)*
On α	9.1 ± 1.1	1.6 ± 1.1	0.18 ± 0.13
On β	0.62 ± 0.073	2.9 ± 1.1	4.7 ± 1.8

strain of about 0.5 mm in a short time of <1 ms. Therefore, this small and fast variation in strain generated and propagated the pulse of the stress. Similarly, in the direction of flow of the pulsejet (direction α in Fig. 4), a shear wave was generated. We calculated the velocity of the shear wave v_e from the isochromatic line images. The result is

$$v_e = 1.30 \pm 0.21\ [\mathrm{m/s}] \quad (\mathrm{N} = 12) \qquad (12)$$

However, at t = 10 ms in Fig. 4, the wave intensity in the β direction is larger than that in the α direction. The variation in strain depends on the velocity of the pulsejet, and the initial jet velocity of 10 m/s was faster than (12). Therefore, at the point of the wave source in the β direction, the variation in strain was generated by a fast jet flow. In contrast, the pulsejet is attenuated as it enters the target. To generate a shear wave in the α direction, the velocity of the pulsejet must be less than (12). Therefore, when the wave in the α direction was generated, the power of the wave source had been attenuated in the α direction. Hence, the wave intensity in direction α was smaller than that in direction β.

To compare shear wave intensities in the α and β directions, we analyzed time variations in shear wave intensity. Fig. 5 shows variations in the isoclinic line at points along the centerline of the pulsejet (Fig. 5(a)) and along the axis perpendicular to the pulsejet (Fig. 5(b)). Using Fig. 5, we analyzed the propagation distance of the shear wave. Figs. 5(a-1) and 5(b-1) show the reaching distance of the pulsejet. We define the propagation distance to be the distance between the reaching position of the pulsejet and the position at which the shear wave intensity is 1/e (Figs. 5(a-1) and 5(b-2)), which is about 0.37. Table 1 shows the propagation distances of the shear wave. The table shows that the propagation distance in the β direction is longer than that in the α direction. To evaluate the scale of the effect of shear wave propagation, we used the ratio of propagation distance to reaching distance. Table 1 shows that the ratio in the β direction is larger than that in the α direction. These results show that the shear wave generated by the pulsejet propagates better in the β direction than in the α direction.

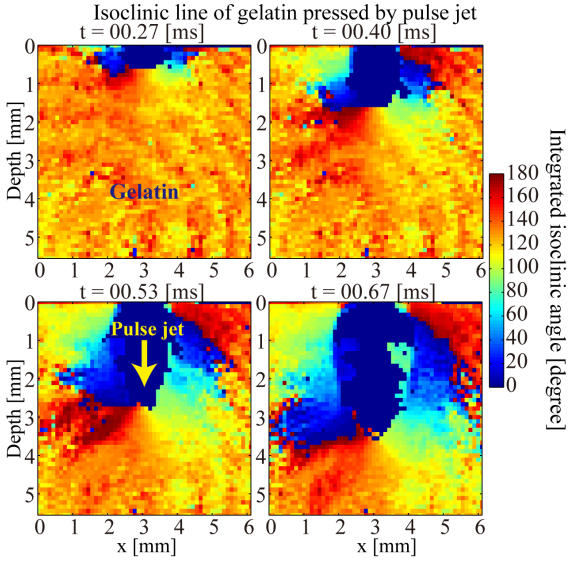

Figure 6. Isoclinic line of gelatin compressed by the pulsejet. These panels show the isoclinic line at selected times after the pulsejet was injected. Blue regions (0°) in center on the x-axis indicate the pulsejet.

Fig. 6 shows that the integrated isoclinic angle radiates around the tip of the pulsejet. The angle does not definitely indicate the direction of the principle stress; however, the symmetry of the pulsejet implies that the stress distribution of the pulsejet has the same axial symmetry. If we measure the axially symmetric stress from the side, the stress projected onto the view plane has point symmetry. In fact, the integrated isoclinic angle in Fig. 6 has point symmetry around the tip of the pulsejet. These results indicate that the pulsejet punctures the gelatin by an axially symmetric stress and enters the gelatin directly.

For a clinical environment, these results show that a pulsejet created by LILJ does not stress deep brain tissue beyond a shallow area. Note that shear stress has the risk of destruction of neurons; thus, since LILJ is used to cure hypophysis, it is important that the effects of needless stress remain small deep in the brain.

V. CONCLUSIONS

To understand the propagation of the stress distribution generated by the pulsejet in LILJ, we used photoelasticity experiments to measure internal stress distributions. The results show that shear wave intensity in the direction parallel to the pulsejet was smaller than that in the perpendicular direction because the wave in the parallel direction was generated by the attenuated jet. We confirmed that the stress distribution around the pulsejet had axial symmetry about the axis along which the pulse was moving.

REFERENCES

[1] T. Ohki, A. Nakagawa, T. Hirano, T. Hashimoto, V. Menezes, H. Jokura, H. Uenohara, Y. Sato, T. Saito, R. Shirane, T. Tominaga, and K. Takayama, "Experimental application of pulsed Ho:YAG laser-induced liquid jet as a novel rigid neuroendoscopic dissection device.," *Lasers Surg. Med.*, vol. 34, no. 3, pp. 227–34, Jan. 2004.

[2] Y. Ogawa, A. Nakagawa, K. Takayama, and T. Tominaga, "Pulsed laser-induced liquid jet for skull base tumor removal with vascular preservation through the transsphenoidal approach: a clinical investigation," *Acta Neurochir.*, vol. 153, no. 4, pp. 823–830, Apr. 2011.

[3] K. Hynynen, N. McDannold, H. Martin, F. A. Jolesz, and N. Vykhodtseva, "The threshold for brain damage in rabbits induced by bursts of ultrasound in the presence of an ultrasound contrast agent (Optison®)," *Ultrasound Med. Biol.*, vol. 29, no. 3, pp. 473–481, Mar. 2003.

[4] K. Ramesh, "Digital Photoelasticity," *Mea. Sci. Technol.*, vol. 11, no. 12, Dec. 2000.

[5] T. Sato, T. Araki, Y. Sasaki, T. Tsuru, T. Tadokoro, and S. Kawakami, "Compact ellipsometer employing a static polarimeter module with arrayed polarizer and wave-plate elements," *Appl. Opt.*, vol. 46, no. 22, pp. 4963–4967, Aug. 2007.

[6] S. Tobita, P. Pinit, and E. Umezaki, "Full-field determination of principal-stress direction from color photoelastic fringes obtained with a semicircular polariscope," *Journal of the Japanese Society for Experimental Mechanics*, vol. 7, pp. 83–88, Jun. 2007. DOI: http://dx.doi.org/10.11395/jjsem.7.s83.

[7] M. L. L. Wijerathne, K. Oguni, and M. Hori, "Tensor field tomography based on 3D photoelasticity," *Mech. Mater.*, vol. 34, no. 9, pp. 533–545, Sep. 2002.